Electron Landau Damping of Turbulence in the Terrestrial Magnetosheath Plasma

A. S. Afshari[1], G. G. Howes[1], C. A. Kletzing[1], D. P. Hartley[1], S. A. Boardsen[2,3]

[1]Department of Physics and Astronomy, The University of Iowa, Iowa City, IA USA

[2]Goddard Planetary Heliophysics Institute, University of Maryland, Baltimore, MD, USA

[3]NASA/GSFC, Greenbelt, MD, USA

Key Points:

- Of the twenty turbulent magnetosheath intervals analyzed, 95% have velocity-space signatures of electron Landau damping.
- Asymmetric bipolar signatures imply that Landau damping is stronger for waves propagating parallel or anti-parallel to the magnetic field.
- Computed electron energization rates suggest that Landau damping is often a major dissipation mechanism of turbulent magnetosheath energy.

Corresponding author: Arya S. Afshari, `arya-afshari@uiowa.edu`

Abstract

High-quality measurements of electromagnetic fields and electron velocity distributions by the Magnetospheric Multiscale (MMS) mission in Earth's magnetosheath present a unique opportunity to characterize heliospheric plasma turbulence and to determine the mechanisms responsible for its dissipation. We apply the field-particle correlation technique to the MMS measurements to identify the dissipation mechanism and quantify the dissipation rate. It is found that 95% of the intervals have velocity-space signatures of electron Landau damping that are quantitatively consistent with linear kinetic theory for the collisionless damping of kinetic Alfvén waves. About 75% of the intervals have asymmetric signatures, implying that often the collisionless damping is stronger for waves propagating one direction along the magnetic field than the other. Nearly half of the samples have the same electron energization rates as order-of-magnitude estimates of the turbulent energy cascade rate, suggesting that electron Landau damping is frequently responsible for the dissipation of magnetosheath turbulent energy.

Plain Language Summary

NASA's Magnetospheric Multiscale (MMS) spacecraft pass through the Earth's magnetosheath (the magnetic boundary layer between the Sun's solar wind and the Earth's magnetosphere) on a regular basis. The data from these magnetosheath traversals are analyzed using a novel diagnostic technique. It is found that Landau damping almost always mediates the transfer of energy between turbulent electromagnetic fields and electrons. Landau damping is analogous to a surfer catching a wave, where the surfer (electron) gains energy from the wave (electric field wave), and in the process removes energy from the wave. Compared to the total cascade rate of energy by the turbulence, in half of the intervals studied, Landau damping appears to dominate the dissipation of the turbulence.

1 Introduction

Heliospheric plasma turbulence plays a key role in transferring the energy of large-scale magnetic field and plasma flow fluctuations to smaller scales where their energy can be dissipated, ultimately leading to plasma heating. Expected to play a key role in solar coronal heating (Cranmer et al., 2015), turbulence has been studied using *in situ* measurements in the solar wind (Tu & Marsch, 1995; Bruno & Carbone, 2013; Kiyani et al., 2015) and planetary magnetospheres (von Papen et al., 2014; Hadid et al., 2015; Tao et al., 2015; Ruhunusiri et al., 2017). These studies have shown that the turbulent power spectrum is embedded in the solar wind and changes through interactions with magnetized bodies. Earth's magnetosheath has been shown to exhibit a power law scaling of the power spectral density (PSD) indicative of turbulence (Chasapis et al., 2015; Vörös et al., 2016; Huang et al., 2017). The regions of the magnetosheath downstream from the bowshock, near the magnetopause, provide the conditions to study this turbulence and the turbulent dissipation mechanisms that transfer the energy from the fields to the plasma particles (Huang et al., 2017; Hadid et al., 2018; Chen et al., 2019).

Various turbulent dissipation mechanisms have been proposed to remove energy from the fluctuating fields and inject it into the plasma particles at kinetic scales. Proposed collisionless energy transfer mechanisms include stochastic heating (Johnson & Cheng, 2001; Chandran et al., 2010; Hoppock et al., 2018; Martinović et al., 2020), cyclotron damping (Hollweg & Markovskii, 2002), and Landau damping (Dobrowolny & Torricelli-Ciamponi, 1985; Leamon et al., 1999; Howes et al., 2008; Schekochihin et al., 2009). The resonant field-particle interaction of Landau damping is a viable mechanism by which particles with an appropriate resonant velocity are energized by the parallel electric field of a kinetic Alfvén wave (KAW) (Klein et al., 2017; Howes et al., 2018). A case study by Chen et al. (2019) made the first direct observation of electron Landau damping in magnetosheath turbulence using the Field-Particle Correlation (FPC) technique (Klein & Howes, 2016; Howes et al., 2017; Klein et al., 2017).

Here the Chen et al. (2019) study is built upon by using the FPC technique to analyze twenty intervals of MMS burst-mode data in the Earth's turbulent magnetosheath. The FPC method is used both to identify signatures of the dissipation mechanism in velocity space, as well as to calculate the total energy density dissipation rate. The purpose of this letter is to use these two results from the FPC method to quantify the contribution of electron Landau damping to the total rate of dissipation of the turbulence.

2 Methodology

2.1 The Field Particle Correlation Technique

The FPC technique utilizes the full 3V velocity-space measurements by the MMS spacecraft to generate a *velocity-space signature* that is characteristic of the kinetic mechanism that governs the dissipation of turbulence and consequent energization of particles (Klein & Howes, 2016; Howes et al., 2017; Klein et al., 2017). Collisions may be neglected on the time scale of the collisionless energy transfer that removes energy from the turbulence, so the Vlasov equation for species s describes the plasma dynamics,

$$\frac{\partial f_s}{\partial t} + \mathbf{v} \cdot \nabla f_s + \frac{q_s}{m_s} \left[\mathbf{E} + \mathbf{v} \times \mathbf{B} \right] \cdot \frac{\partial f_s}{\partial \mathbf{v}} = 0. \tag{1}$$

The Vlasov equation is multiplied by $m_s v^2/2$ to obtain the time evolution of the 3D-3V phase-space energy density, $w_s(\mathbf{r}, \mathbf{v}, t) = m_s v^2 f_s(\mathbf{r}, \mathbf{v}, t)/2$,

$$\frac{\partial w_s}{\partial t} = -\mathbf{v} \cdot \nabla w_s - q_s \frac{v^2}{2} \mathbf{E} \cdot \frac{\partial f_s}{\partial \mathbf{v}} - q_s \frac{v^2}{2} (\mathbf{v} \times \mathbf{B}) \cdot \frac{\partial f_s}{\partial \mathbf{v}}. \tag{2}$$

When (2) is integrated over all 3D-3V phase-space, yielding the rate of change of total energy $\mathcal{W}_s$ of species s, only the electric field term is non-zero (Howes et al., 2017), so any net change in energy is due to the electric field. Since it is $E_\parallel$ that energizes particles in Landau damping, the rate of electron energization by Landau damping can be assessed by taking the unnormalized correlation

$$C_{E_\parallel}(\mathbf{v}, t, \tau) = C \left(-q_s \frac{v_\parallel^2}{2} \frac{\partial f_e(\mathbf{r_0}, \mathbf{v}, t)}{\partial v_\parallel}, E_\parallel(\mathbf{r_0}, t) \right). \tag{3}$$

The correlation is taken over a sufficiently long interval τ to average out the oscillatory energy transfer associated with undamped wave motion, exposing the smaller amplitude signal of secular energization (Klein & Howes, 2016; Howes et al., 2017). Integrating over the velocity-space dimension perpendicular to the local magnetic field yields the reduced parallel velocity-space signature $C_{E_\parallel}(v_\parallel, t, \tau)$.

The form of $C_{E_\parallel}(v_\parallel, t, \tau)$ for Landau damping is illustrated in Figure 1, where (a) the perturbation of $f(v_\parallel)$, associated with a KAW travelling up the magnetic field with phase velocity $\omega/k_\parallel$, leads to (b) an instantaneous correlation $C_{E_\parallel}(v_\parallel, t, 0)$ dominated by oscillatory energy transfer in time about the resonant phase velocity $\omega/k_\parallel$ (vertical dashed black line). By taking the average over a sufficiently long correlation interval, here equal to the wave period $\tau = T$, $C_{E_\parallel}(v_\parallel, t, \tau)$ becomes steady in time, and (d) its time average yields the characteristic bipolar form of the velocity-space signature for Landau damping, where $C_{E_\parallel}(v_\parallel)$ crosses from negative to positive at the resonant velocity (Klein & Howes, 2016; Howes et al., 2017; Howes, 2017; Klein et al., 2017; Howes et al., 2018; Klein et al., 2020). Physically, the net effect of the resonant interaction with $E_\parallel$ is that particles with $v_\parallel < \omega/k_\parallel$ are accelerated to $v_\parallel > \omega/k_\parallel$, leading to a net loss of phase-energy density below, and an increase above, the resonance. This leads to the bipolar velocity-space signature seen in Figure 1(d).

To avoid difficulties with taking velocity-space derivatives in 3V velocity-space, the procedure of Chen et al. (2019) is followed and the alternative correlation $C'_{E_\parallel}(\mathbf{v}, t, \tau) = C(q_e v_\parallel f_e, E_\parallel)$ in 3V space is calculated. After integration of $C'_{E_\parallel}$ over the perpendicular velocity coordinates, $C_{E_\parallel}(v_\parallel)$ is obtained by computing

$$C_{E_\parallel}(v_\parallel) = -\frac{v_\parallel}{2}\frac{\partial C'_{E_\parallel}(v_\parallel)}{\partial v_\parallel} + \frac{C'_{E_\parallel}(v_\parallel)}{2}. \tag{4}$$

2.2 Selection of Intervals

MMS magnetosheath intervals are identified through the use of the orbit plots, Fluxgate Magnetometer (FGM) data (Russell et al., 2016), and Fast Plasma Investigation (FPI) density

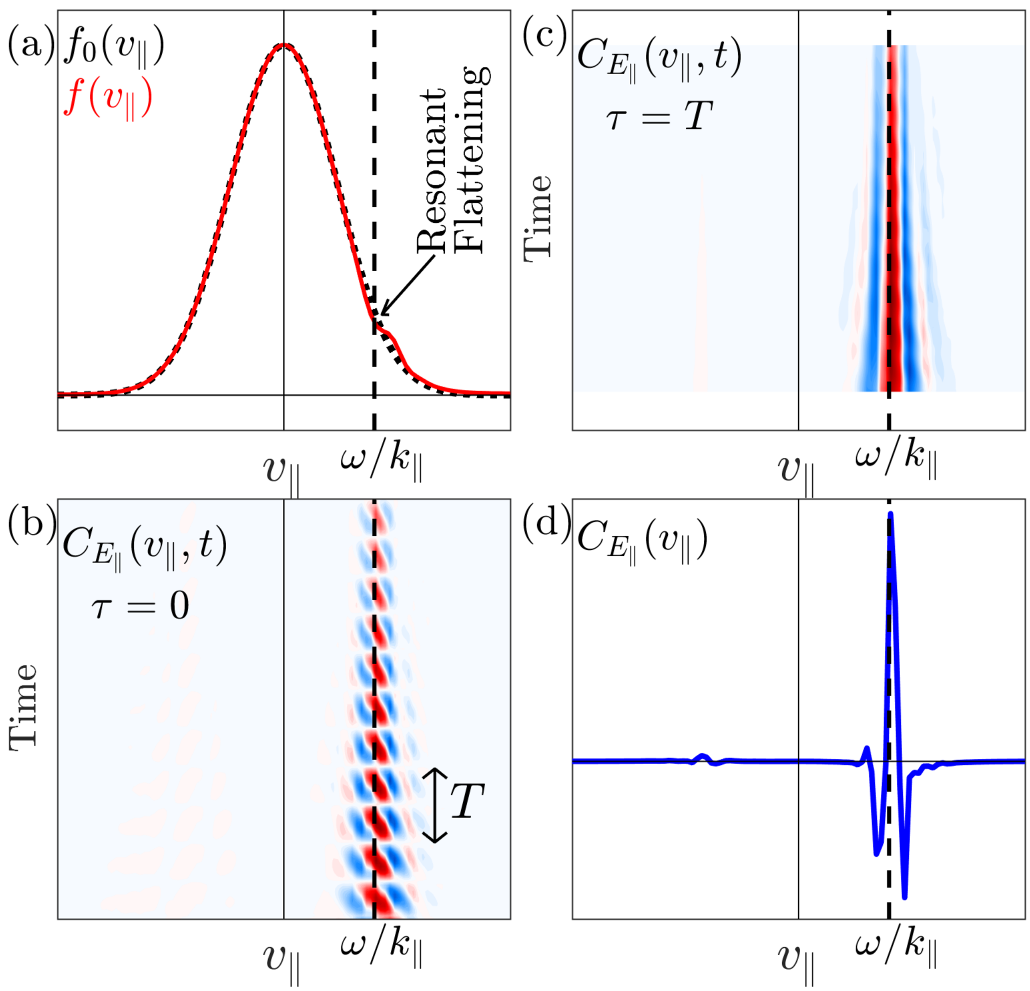

Figure 1: (a) Landau damping leads to a flattening of the velocity distribution $f(v_\parallel)$ at the resonant phase velocity $v_\parallel = \omega/k_\parallel$. (b) An instantaneous field-particle correlation with $\tau = 0$ yields a signature in $v_\parallel$ that oscillates in time. (c) Averaging over an interval equal to the wave period $\tau = T$ leads to a persistent velocity-space signature. (d) The time-averaged correlation $C_{E_\parallel}(v_\parallel)$ exhibits a bipolar signature, crossing from negative to positive at the resonant velocity, a distinguishing characteristic of Landau damping.

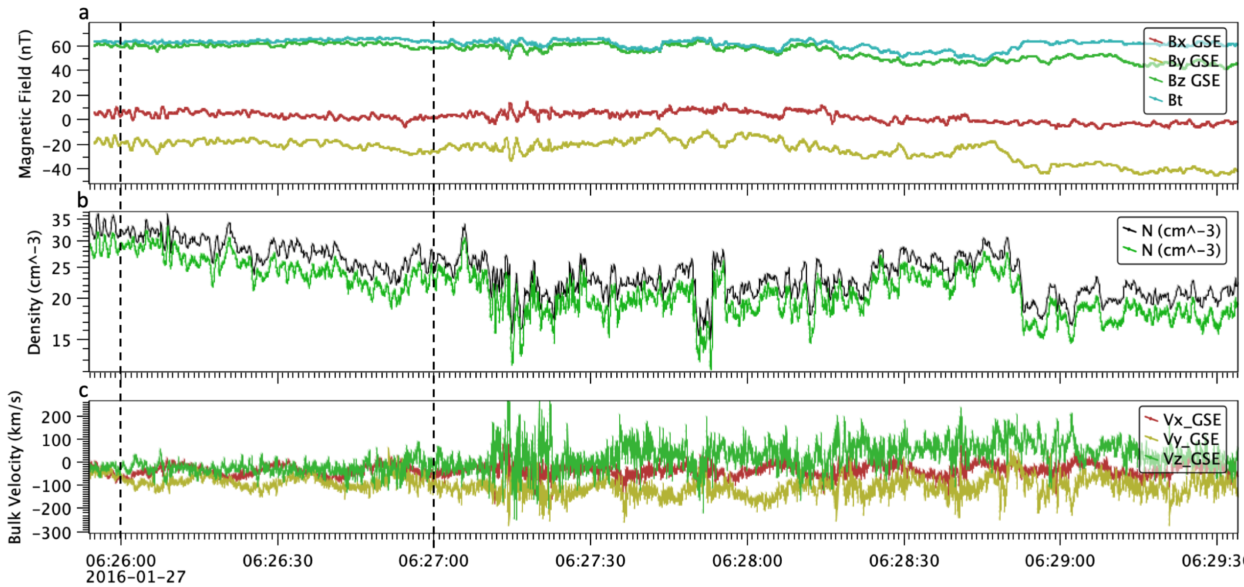

Figure 2: Interval during 2016-01-27 from MMS 1: (a) The magnetic field in geocentric-solar-ecliptic (GSE) coordinates, (b) the ion (black) and electron (green) densities from FPI moments, and (c) the electron bulk velocity.

data (Pollock et al., 2016). The magnetosheath is defined as the layer between the bowshock and the magnetopause, with generally higher temperatures and higher densities than the solar wind and magnetospheric plasmas. Intervals when MMS is downstream of the bowshock, close to the magnetopause, are selected. Time-averaging over the correlation interval τ in magnetic field-aligned coordinates ($v_\parallel$, $v_\perp$) requires an accurate definition of the equilibrium magnetic field $\mathbf{B}_0$. This is facilitated when the magnetic field direction is relatively constant with no discontinuities. Magnetosheath intervals with relatively constant magnetic field direction, electron density, and ion density, as well as no velocity shears are selected. Figure 2 shows a representation of a burst mode interval from the MMS 1 spacecraft during 2016-01-27 at 06:25:54 that satisfies the selection criteria, taken on an inbound pass, closer to the magnetopause than the bowshock. We analyze the $T = 60$ s interval from 06:26:00–06:27:00 (sample 17 in this study) because it contains (a) a steady ambient field, (b) a density typical of the magnetosheath, and (c) no velocity shears.

2.3 Data Analysis

The MMS measurements employed here are the electron velocity distributions and moments from FPI with a 30 ms cadence (Pollock et al., 2016), the electric field double probes measurements sampled at 8192 Hz (Ergun et al., 2016; Lindqvist et al., 2016), and FGM magnetic field measurements sampled at 128 Hz (Ergun et al., 2016). We follow the same FPC analysis procedure as outlined by Chen et al. (2019). The equilibrium magnetic field is calculated by averaging over the full sample duration T, $\mathbf{B}_0 = \langle \mathbf{B} \rangle_T$. Velocity measurements are transformed to the frame of the mean electron bulk flow, $\mathbf{U}_{0e} = \langle \mathbf{U}_e \rangle_T$, with corrections applied in the energy bins to account for any acceleration due to the charged spacecraft. The velocity coordinates are then projected onto a field-aligned coordinate system, $(v_\parallel, v_\perp)$. Electric field measurements are Lorentz transformed (Chen et al., 2011; Howes et al., 2014) to the same frame, downsampled to 30 ms to match the cadence of FPI, then projected onto $\mathbf{B}_0$ to obtain $E_\parallel(t)$.

To accentuate the signal of secular electron energization using the FPC method, two measures are taken. First, to suppress the large-amplitude signal of oscillatory energy transfer by large-scale electric fields, $E_\parallel(t)$ is high pass filtered at 1 Hz to obtain $\overline{E}_\parallel(t)$. Second, to eliminate the contribution to $\partial w_e/\partial t$ associated with the equilibrium electron velocity distribution, $f_0(v_\parallel, v_\perp) = \langle f(v_\parallel, v_\perp, t) \rangle_T$, which integrates to zero over velocity (Howes et al., 2017), we compute $C'_{E_\parallel}(v_\parallel, v_\perp, t, \tau)$ using the perturbed velocity distribution $\delta f(v_\parallel, v_\perp, t) = f(v_\parallel, v_\perp, t) - f_0(v_\parallel, v_\perp)$ (Chen et al., 2019). The resulting correlation $C'_{E_\parallel}(v_\parallel, v_\perp, t, \tau) = C(q_e v_\parallel \delta f, \overline{E}_\parallel)$ is then integrated over the perpendicular velocity coordinates and the azimuthal angle (ϕ) with respect to $\mathbf{B}_0$ to obtain

$$C'_{E_\parallel}(v_\parallel, t, \tau) = \int dv_\perp \int_0^{2\pi} v_\perp d\phi C'_{E_\parallel}(v_\parallel, v_\perp, t, \tau). \tag{5}$$

Finally, (4) is used to obtain the final reduced parallel correlation $C_{E_\parallel}(v_\parallel, t, \tau)$, from which the velocity-space signature of electron Landau damping as a function of time t and correlation interval τ is sought. In addition, one may integrate $C_{E_\parallel}(v_\parallel, t, \tau)$ over parallel velocity to

Sample	Date	Interval	τ (s)	Electron β	Ion β	Signature	Electron Energization Rate (x 10^{-12} J $\mathrm{m}^{-3}\mathrm{s}^{-1}$)	Theoretical Cascade Rate (x 10^{-12} J $\mathrm{m}^{-3}\mathrm{s}^{-1}$)	Ratio
00	2015-10-16	09:24:11 - 09:25:21	70	0.08	0.83	S	5.8	2.6	2.2
02	2016-01-12	07:24:38 - 07:25:45	77	0.05	0.75	A	1.7	23	0.075
03	2016-01-13	04:56:40 - 04:57:07	27	0.13	1.12	A	0.42	43	0.0099
04	2016-01-14	05:30:26 - 05:30:51	24	0.15	1.14	A	3.6	33	0.11
05	2016-01-15	02:29:52 - 02:31:10	78	0.62	4.26	S	1.5	4.4	0.33
06	2016-01-16	07:12:20 - 07:13:00	40	0.14	1.11	A	14	30	0.48
07	2016-01-17	01:46:28 - 01:46:43	15	0.11	0.64	A	1.0	34	0.031
08	2016-01-18	00:50:55 - 00:51:57	62	0.17	0.87	A	17	16	1.1
09	2016-01-19	07:24:20 - 07:24:40	20	0.85	5.21	N	1.9	31	0.060
10	2016-01-20	02:52:00 - 02:54:30	150	0.32	0.99	A	0.65	28	0.023
11	2016-01-21	03:51:45 - 03:52:17	32	0.60	2.10	A	0.79	15	0.051
12	2016-01-22	00:19:15 - 00:19:54	39	1.20	8.67	A	1.5	9.3	0.16
13	2016-01-23	02:08:20 - 02:09:42	82	0.77	4.19	A	2.5	33	0.077
14	2016-01-24	04:29:54 - 04:30:43	49	0.25	1.69	A	1.3	5.1	0.26
15	2016-01-25	02:18:00 - 02:18:20	20	0.45	2.38	A	23	28	0.82
16	2016-01-26	00:34:25 - 00:34:45	20	0.21	1.41	S	1.8	8.1	0.23
17	2016-01-27	06:26:00 - 06:27:00	60	0.04	0.34	S	7.6	9.0	0.85
18	2016-01-28	06:05:15 - 06:05:47	32	0.10	0.63	S	52	350	0.15
19	2016-01-29	23:55:15 - 23:55:40	25	0.16	1.55	S	14	49	0.28
20	2016-01-30	03:33:00 - 03:34:10	70	0.04	0.40	A	0.12	1.4	0.090

Table 1: Table of analyzed MMS intervals (all from MMS 1, except for sample 00 from MMS 3), including electron energization rates $\partial W_e \partial t$ from the integrated experimental measurements and the theoretically estimated turbulent cascade rate ϵ. Qualitative signatures are symmetric (S), asymmetric (A), or no clear signature (N). The Ratio column gives $(\partial W_e/\partial t)/\epsilon$.

obtain the rate of change of spatial energy density W_e due to $E_\parallel$ at the spacecraft position $\mathbf{r}_0$, $\partial W_e(\mathbf{r}_0, t)/\partial t$.

3 Results

Twenty samples listed in Table 1, including sample 00 from Chen et al. (2019), were analyzed to seek the characteristic bipolar velocity-space signatures of electron Landau damping and their evolution over time by varying the correlation interval τ. We evaluate the evolution of the electron energization with timestack plots of the parallel field-particle correlation $C_{E_\parallel}(v_\parallel, t)$ over the sample duration in Figure 3(a) for sample 17 with $\tau = 3.96$ s and (c) for sample 08 with $\tau = 1.98$ s. The time-averaged parallel correlations, taken over the full sample duration $\tau = T$, for these two intervals are plotted in (b) and (d). The timestack plots show that while the phase-space energy density transfer rate as a function of $v_\parallel$ varies in time, when its amplitude is significant, it generally has the bipolar form characteristic of the Landau resonance about a parallel velocity $v_\parallel/v_{th,e} \sim 1$. Furthermore, the more clear bipolar velocity-space signatures in the time-averaged correlations, when looking at the timestack plots, are generally found to be more persistent in time.

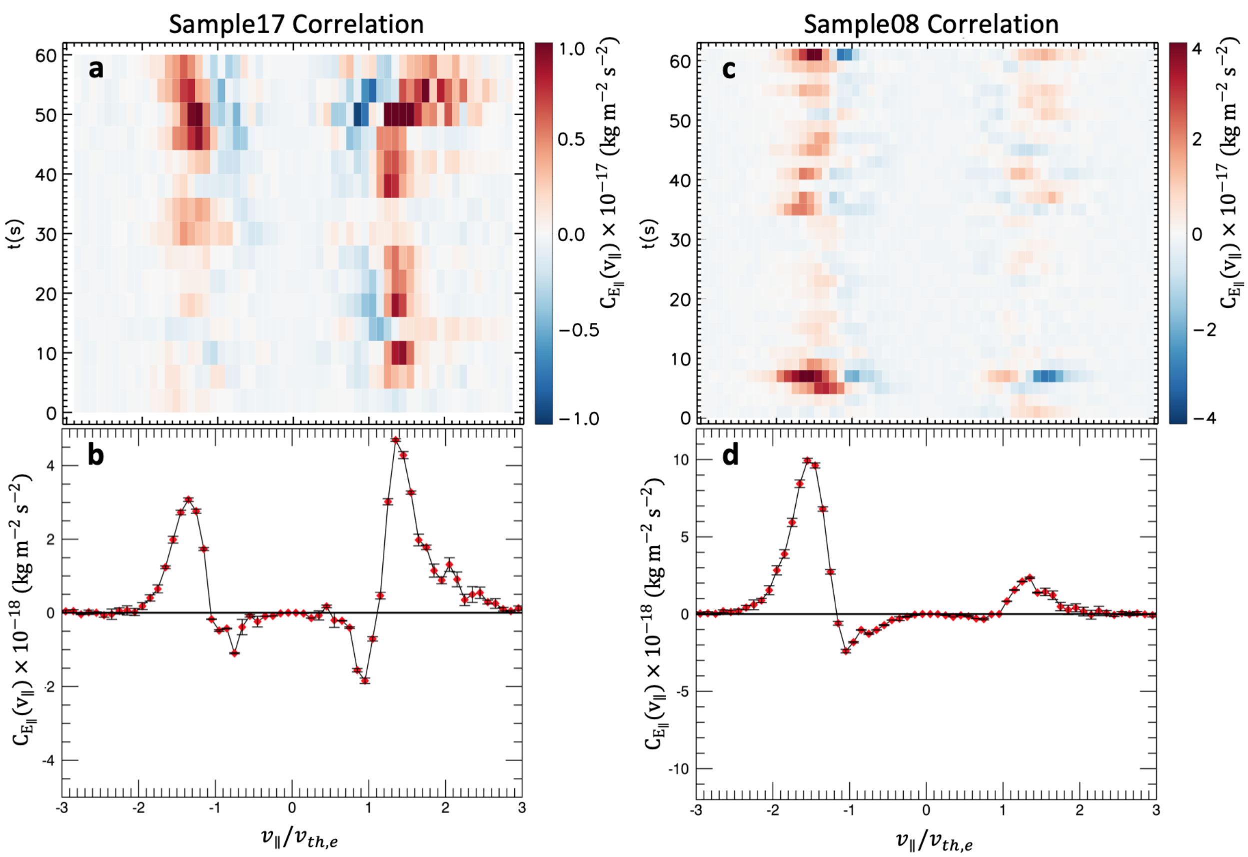

Figure 3: Timestack plots of $C_{E_\parallel}(v_\parallel, t)$ (a) for sample 17 with $\tau = 4$ s and (c) for sample 08 with $\tau = 2$ s and time-averaged correlation $C_{E_\parallel}(v_\parallel)$ with $\tau = T$ for (b) sample 17 and (d) sample 08.

Linear kinetic theory predicts that, under the magnetosheath plasma parameters, the resonant parallel phase velocites of KAWs generally satisfy $\omega/k_\parallel v_{th,e} = v_\parallel/v_{th,e} \sim 1$ when the collisionless damping becomes strong as $k_\perp \rho_e \to 1$. Therefore, the velocities of the zero crossings in the time-averaged, parallel velocity-space signatures correspond quantitatively to the resonant velocities expected for electron Landau damping.

In Figure 4, the time-averaged, parallel field-particle correlations $C_{E_\parallel}(v_\parallel)$ for all twenty samples with $\tau = T$ are plotted. Five of the samples (05, 16, 17, 18, 19) show a velocity-space signature that is approximately symmetric about $v_\parallel$, qualitatively similar to sample 00 from Chen et al. (2019), but it appears that this result is not typical of all samples. However, all plots in Figure 4 but sample 09 show a clear bipolar velocity-space signature at either $v_\parallel/v_{th,e} \sim 1$ or $v_\parallel/v_{th,e} \sim -1$, or both. Landau resonant damping of KAWs energizes particles moving approximately at the wave phase velocity *in the direction of wave propagation*, as illustrated in Figure 1. Therefore, we interpret the 13 examples of asymmetric velocity-space signatures in Figure 4 to indicate that more wave-energy flux is being damped in one-direction along $\mathbf{B}_0$ than the other. In fact, a recent numerical simulation of the Chen et al. (2019) interval finds that the velocity-space signatures of electron Landau damping can have a variety of qualitative appearances (Horvath et al., 2020), similar to what is observed in Figure 4. In summary, it is found that 19 of the 20 intervals, representing 95% of the cases in Figure 4, show clear evidence that electron Landau damping is playing a key role in removing energy from the turbulent fluctuations in the magnetosheath.

With its ubiquity in magnetosheath turbulence established, the fraction of the turbulent dissipation governed by electron Landau damping is next identified. Integrating $C_{E_\parallel}(v_\parallel)$ over $v_\parallel$ yields the rate of change of electron spatial energy density due to $E_\parallel$ at the point of observation, $\partial W_e(\mathbf{r}_0, t)/\partial t$, with the results listed in Table 1. Note that, although the reversible nature of collisionless energy transfer allows for negative values that indicate the transfer of energy from electrons to $E_\parallel$, in all samples a net transfer of energy to the electrons is found. For each sample, this electron energization rate is compared with a theoretically estimated tur-

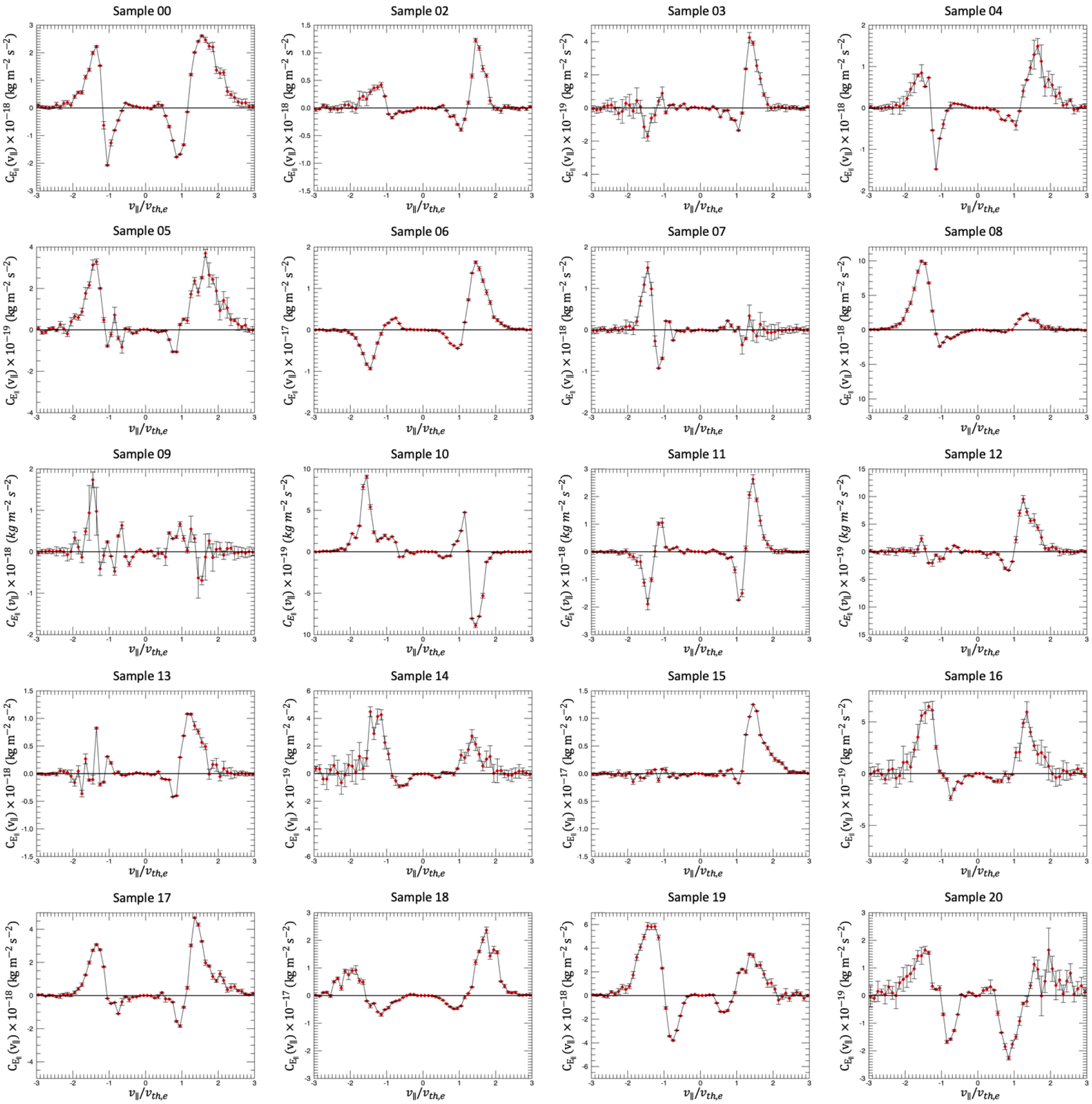

Figure 4: Time-averaged, parallel field-particle correlations $C_{E_\parallel}(v_\parallel)$ for all twenty samples with $\tau = T$ from Table 1.

bulent energy cascade rate ϵ in the inertial range from a cascade model (Howes et al., 2008, 2011) given by

$$\epsilon \sim \frac{\text{Energy Density}}{\text{Cascade Time}} = \frac{n_0 m_p U_\perp^2}{1/(k_\perp U_\perp)} = n_0 m_p \left(\frac{2\pi f}{v_{\perp,sc}}\right) \frac{[\delta \hat{B}_\perp(f)]^3}{(\mu_0 n_0 m_p)^{3/2}}. \tag{6}$$

Here the turbulent energy density includes both kinetic and magnetic contributions which are assumed equal for Alfvénic turbulence, $\delta\hat{B}_\perp(f)$ is the amplitude of magnetic field fluctuations at the inertial range frequency $f = 0.2$ Hz computed from the time series as the increment with lag $t = 5$ s. The Taylor hypothesis (Taylor, 1938) is assumed to estimate $k_\perp$ as the factor in parentheses where $v_{\perp,sc}$ is the component of the spacecraft velocity perpendicular to $\mathbf{B}_0$ (Howes et al., 2014) and a typical anisotropy $k_\parallel \ll k_\perp$ is assumed (Sahraoui et al., 2010). The MHD Alfvén wave eigenfunction is used to estimate $U_\perp = \delta B_\perp v_A/B_0$. The resulting estimates for the turbulent energy cascade rate ϵ, listed in Table 1, are plotted against the measured electron energization rates $\partial W_e(\mathbf{r}_0, t)/\partial t$ in Figure 5.

The solid line in Figure 5 indicates $\partial W_e/\partial t = \epsilon$, meaning the measured rate of energization by electron Landau damping is sufficient to remove all of the energy from the turbulent cascade. Theoretically, however, the cascade rate estimate, derived from a scaling theory, is only an order-of-magnitude calculation, so dotted lines at factors of 3 above and below indicate the range of accuracy of this order-of-magnitude estimate for ϵ. Our key result is that nearly half of the samples have measured electron energization rates that fall within the order-of-magnitude estimate for ϵ, meaning that electron Landau damping is frequently a major, if not the dominant, mechanism responsible for the dissipation of turbulent energy in Earth's magnetosheath.

4 Conclusion

An FPC analysis of a selection of twenty intervals of turbulence from the magnetosheath near the subsolar point has been performed to find that 95% of the intervals have velocity-space signatures of electron Landau damping. The resonant zero crossings of the bipolar velocity-space signatures are quantitatively consistent with the theoretical expectation for KAWs that the resonant phase velocities have values $\omega/k_\parallel v_{th,e} \sim 1$ as the collisionless damping becomes strong. These findings confirm the first definitive identification of electron Landau damping in the magnetosheath by Chen et al. (2019). However, it is found that only

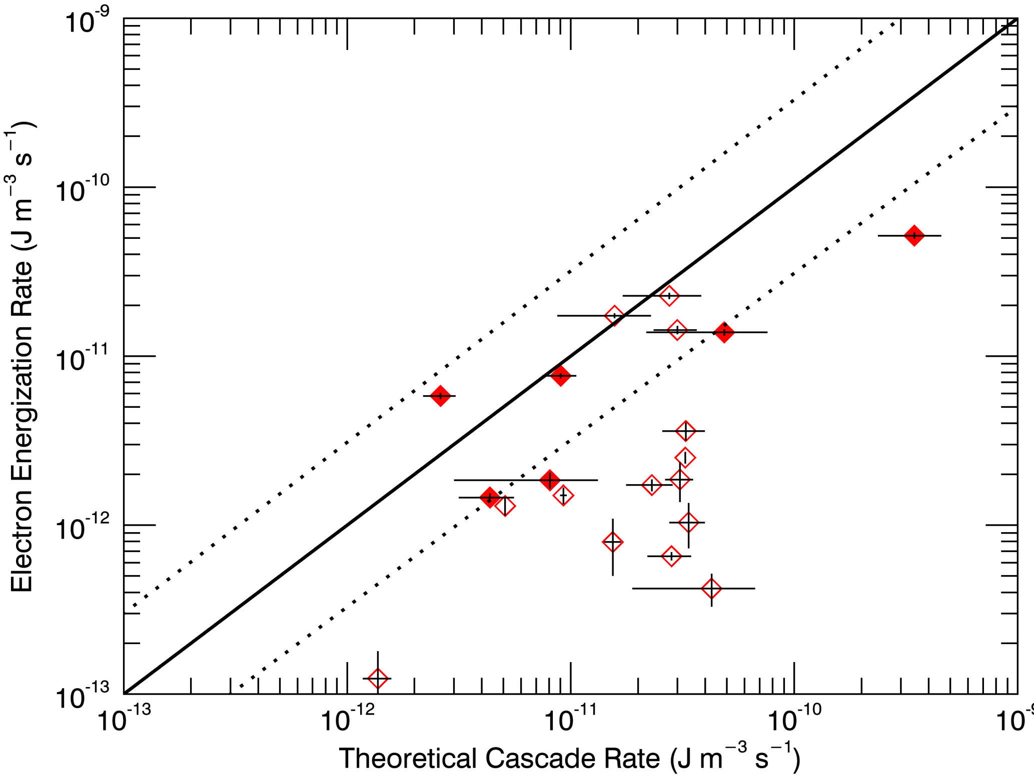

Figure 5: The electron energization rate $\partial W_e/\partial t$ vs. theoretical cascade rate ϵ, where the solid line indicates $\partial W_e/\partial t = \epsilon$ and the dotted lines indicate the range of the order-of-magnitude estimate of ϵ. Solid diamonds mark symmetric signatures, open diamonds asymmetric.

about one quarter of the intervals produce symmetric bipolar signatures at $v_\parallel/v_{th,e} \sim \pm 1$ as seen in Chen et al. (2019), indicating that typically one finds that the damping of waves in one direction along $\mathbf{B}_0$ exceeds that in the other direction, a finding consistent with a recent kinetic numerical simulation of magnetosheath turbulence (Horvath et al., 2020). Relative to the theoretically estimated turbulent energy cascade rate ϵ, it is found that nearly half of the samples have electron energization rates by Landau damping that account for the dissipation of a significant fraction, if not a majority, of the turbulent energy. In fact, the measured rates of electron energizaton by Landau damping span the range $\partial W_e/\partial t \in [10^{-13}, 10^{-11}]$ Jm^{-3}s^{-1}, values that are much higher than the mean energy cascade rates of $\epsilon \lesssim 4 \times 10^{-14}$ $\mathrm{Jm^{-3}s^{-1}}$ for Alfvénic cases and $\epsilon \lesssim 6 \times 10^{-13}$ $\mathrm{Jm^{-3}s^{-1}}$ for magnetosonic cases reported in Hadid et al. (2018) for magnetosheath turbulence.

Future work will relax the restriction of the FPC analysis to intervals with relatively constant $\mathbf{B}_0$ and no velocity shears, enabling a larger statistical sample of MMS burst-mode intervals to be analyzed and to rule out selection bias in these results. In addition, the parallel Poynting energy flux will be examined in the cases with asymmetric signatures to test the interpretation that the wave damping is stronger for waves in one direction along $\mathbf{B}_0$ than the other.

Acknowledgments

This work was performed under the support of University of New Hampshire contract 06-0002 under NASA Prime contract NNG04EB99C. G. G. H. was supported by NASA grants 80NSSC18K0643 and 80NSSC18K1371. A.S.A. would like to thank Jason Shuster and Tak Chu Li for the useful discussions. The data used in this research is available to the public via the MMS Science Data Center (https://lasp.colorado.edu/mms/sdc/public/).

References

Bruno, R., & Carbone, V. (2013, May). The Solar Wind as a Turbulence Laboratory. *Living Reviews in Solar Physics*, *10*(1), 2. doi: 10.12942/lrsp-2013-2

Chandran, B. D. G., Li, B., Rogers, B. N., Quataert, E., & Germaschewski, K. (2010, September). Perpendicular Ion Heating by Low-frequency Alfvén-wave Turbulence in the Solar Wind. , *720*(1), 503-515. doi: 10.1088/0004-637X/720/1/503

Chasapis, A., Retinò, A., Sahraoui, F., Vaivads, A., Khotyaintsev, Y. V., Sundkvist, D., . . . Canu, P. (2015, May). Thin Current Sheets and Associated Electron Heating in Turbulent Space Plasma. , *804*(1), L1. doi: 10.1088/2041-8205/804/1/L1

Chen, C. H. K., Bale, S. D., Salem, C., & Mozer, F. S. (2011, August). Frame Dependence of the Electric Field Spectrum of Solar Wind Turbulence. *Astrophys. J. Lett.*, *737*, L41. doi: 10.1088/2041-8205/737/2/L41

Chen, C. H. K., Klein, K. G., & Howes, G. G. (2019, February). Evidence for electron Landau damping in space plasma turbulence. *Nature Communications*, *10*, 740. doi: 10.1038/s41467-019-08435-3

Cranmer, S. R., Asgari-Targhi, M., Miralles, M. P., Raymond, J. C., Strachan, L., Tian, H., & Woolsey, L. N. (2015, April). The role of turbulence in coronal heating and solar wind expansion. *Philosophical Transactions of the Royal Society of London Series A*, *373*(2041), 20140148-20140148. doi: 10.1098/rsta.2014.0148

Dobrowolny, M., & Torricelli-Ciamponi, G. (1985, January). Alfven wave dissipation in the solar wind. , *142*(2), 404-410.

Ergun, R. E., Tucker, S., Westfall, J., Goodrich, K. A., Malaspina, D. M., Summers, D., ... Cully, C. M. (2016, March). The Axial Double Probe and Fields Signal Processing for the MMS Mission. , *199*(1-4), 167-188. doi: 10.1007/s11214-014-0115-x

Hadid, L. Z., Sahraoui, F., Galtier, S., & Huang, S. Y. (2018, January). Compressible Magnetohydrodynamic Turbulence in the Earth's Magnetosheath: Estimation of the Energy Cascade Rate Using in situ Spacecraft Data. , *120*(5), 055102. doi: 10.1103/PhysRevLett.120.055102

Hadid, L. Z., Sahraoui, F., Kiyani, K. H., Retinò, A., Modolo, R., Canu, P., ... Dougherty, M. K. (2015, November). Nature of the MHD and Kinetic Scale Turbulence in the Magnetosheath of Saturn: Cassini Observations. *Astrophys. J. Lett.*, *813*(2), L29. doi: 10.1088/2041-8205/813/2/L29

Hollweg, J. V., & Markovskii, S. A. (2002). Cyclotron resonances of ions with obliquely propagating waves in coronal holes and the fast solar wind. *Journal of Geophysical Research: Space Physics*, *107*(A6), SSH 1-1-SSH 1-7. Retrieved from https://agupubs.onlinelibrary.wiley.com/doi/abs/10.1029/2001JA000205 doi: 10.1029/2001JA000205

Hoppock, I. W., Chandran, B. D. G., Klein, K. G., Mallet, A., & Verscharen, D. (2018, December). Stochastic proton heating by kinetic-Alfvén-wave turbulence in moderately high-β plasmas. *Journal of Plasma Physics*, *84*(6), 905840615. doi: 10.1017/S0022377818001277

Horvath, S. A., Howes, G. G., & McCubbin, A. J. (2020). Electron Landau Damping of Kinetic Alfvén Waves in Simulated Magnetosheath Turbulence. *Phys. Plasmas*. (submitted)

Howes, G. G. (2017). A prospectus on kinetic heliophysics. *Phys. Plasmas*, *24*(5), 055907. doi: 10.1063/1.4983993

Howes, G. G., Cowley, S. C., Dorland, W., Hammett, G. W., Quataert, E., & Schekochihin, A. A. (2008, May). A model of turbulence in magnetized plasmas: Implications for the dissipation range in the solar wind. *Journal of Geophysical Research (Space Physics)*, *113*(A5), A05103. doi: 10.1029/2007JA012665

Howes, G. G., Klein, K. G., & Li, T. C. (2017, February). Diagnosing collisionless energy transfer using field-particle correlations: Vlasov-Poisson plasmas. *J. Plasma Phys.*, *83*(1), 705830102. doi: 10.1017/S0022377816001197

Howes, G. G., Klein, K. G., & TenBarge, J. M. (2014, July). Validity of the Taylor Hypothesis for Linear Kinetic Waves in the Weakly Collisional Solar Wind. , *789*(2), 106. doi: 10.1088/0004-637X/789/2/106

Howes, G. G., McCubbin, A. J., & Klein, K. G. (2018, February). Spatially localized particle energization by Landau damping in current sheets produced by strong Alfvén wave collisions. *J. Plasma Phys.*, *84*(1), 905840105. doi: 10.1017/S0022377818000053

Howes, G. G., Tenbarge, J. M., & Dorland, W. (2011, October). A weakened cascade model for turbulence in astrophysical plasmas. *Physics of Plasmas*, *18*(10), 102305-102305. doi: 10.1063/1.3646400

Huang, S. Y., Hadid, L. Z., Sahraoui, F., Yuan, Z. G., & Deng, X. H. (2017, February).

On the Existence of the Kolmogorov Inertial Range in the Terrestrial Magnetosheath Turbulence. , *836*(1), L10. doi: 10.3847/2041-8213/836/1/L10

Johnson, J. R., & Cheng, C. Z. (2001, January). Stochastic ion heating at the magnetopause due to kinetic Alfvén waves. , *28*(23), 4421-4424. doi: 10.1029/2001GL013509

Kiyani, K. H., Osman, K. T., & Chapman, S. C. (2015, April). Introduction: Dissipation and heating in solar wind turbulence: from the macro to the micro and back again. *Philosophical Transactions of the Royal Society of London Series A*, *373*, 40155.

Klein, K. G., & Howes, G. G. (2016, August). Measuring Collisionless Damping in Heliospheric Plasmas using Field-Particle Correlations. *Astrophysical Journal Letters*, *826*, L30. doi: 10.3847/2041-8205/826/2/L30

Klein, K. G., Howes, G. G., & Tenbarge, J. M. (2017, August). Diagnosing collisionless energy transfer using field-particle correlations: gyrokinetic turbulence. *Journal of Plasma Physics*, *83*(4), 535830401. doi: 10.1017/S0022377817000563

Klein, K. G., Howes, G. G., TenBarge, J. M., & Valentini, F. (2020). Diagnosing collisionless energy transfer using field-particle correlations: Alfvén-ion cyclotron turbulence. *Journal of Plasma Physics*, *86*, 905860402. doi: 10.1017/S0022377820000689

Leamon, R. J., Smith, C. W., Ness, N. F., & Wong, H. K. (1999). Dissipation range dynamics: Kinetic alfvn waves and the importance of e. *Journal of Geophysical Research: Space Physics*, *104*(A10), 22331-22344. Retrieved from https://agupubs.onlinelibrary.wiley.com/doi/abs/10.1029/1999JA900158 doi: 10.1029/1999JA900158

Lindqvist, P. A., Olsson, G., Torbert, R. B., King, B., Granoff, M., Rau, D., … Tucker, S. (2016, March). The Spin-Plane Double Probe Electric Field Instrument for MMS. , *199*(1-4), 137-165. doi: 10.1007/s11214-014-0116-9

Martinović, M. M., Klein, K. G., Kasper, J. C., Case, A. W., Korreck, K. E., Larson, D., … MacDowall, R. J. (2020, February). The Enhancement of Proton Stochastic Heating in the Near-Sun Solar Wind. , *246*(2), 30. doi: 10.3847/1538-4365/ab527f

Pollock, C., Moore, T., Jacques, A., Burch, J., Gliese, U., Saito, Y., … Zeuch, M. (2016, March). Fast Plasma Investigation for Magnetospheric Multiscale. , *199*(1-4), 331-406. doi: 10.1007/s11214-016-0245-4

Ruhunusiri, S., Halekas, J. S., Espley, J. R., Mazelle, C., Brain, D., Harada, Y., … Howes, G. G. (2017, January). Characterization of turbulence in the Mars plasma environment with MAVEN observations. *Journal of Geophysical Research (Space Physics)*, *122*(1), 656-674. doi: 10.1002/2016JA023456

Russell, C. T., Anderson, B. J., Baumjohann, W., Bromund, K. R., Dearborn, D., Fischer, D., … Richter, I. (2016, March). The Magnetospheric Multiscale Magnetometers. , *199*(1-4), 189-256. doi: 10.1007/s11214-014-0057-3

Sahraoui, F., Goldstein, M. L., Belmont, G., Canu, P., & Rezeau, L. (2010, September). Three Dimensional Anisotropic k Spectra of Turbulence at Subproton Scales in the Solar Wind. *Phys. Rev. Lett.*, *105*(13), 131101. doi: 10.1103/PhysRevLett.105.131101

Schekochihin, A. A., Cowley, S. C., Dorland, W., Hammett, G. W., Howes, G. G., Quataert, E., & Tatsuno, T. (2009, May). ASTROPHYSICAL GYROKINETICS: KINETIC AND FLUID TURBULENT CASCADES IN MAGNETIZED WEAKLY COLLISIONAL PLASMAS. *The Astrophysical Journal Supplement Series*, *182*(1), 310–377. Retrieved from `https://doi.org/10.1088%2F0067-0049%2F182%2F1%2F310` doi: 10.1088/0067-0049/182/1/310

Tao, C., Sahraoui, F., Fontaine, D., Patoul, J., Chust, T., Kasahara, S., & Retinò, A. (2015, April). Properties of Jupiter's magnetospheric turbulence observed by the Galileo spacecraft. *Journal of Geophysical Research (Space Physics)*, *120*(4), 2477-2493. doi: 10.1002/2014JA020749

Taylor, G. I. (1938). The Spectrum of Turbulence. *Proc. Roy. Soc. A*, *164*, 476–490.

Tu, C. Y., & Marsch, E. (1995). *MHD structures, waves and turbulence in the solar wind: observations and theories*.

von Papen, M., Saur, J., & Alexandrova, O. (2014, April). Turbulent magnetic field fluctuations in Saturn's magnetosphere. *Journal of Geophysical Research (Space Physics)*, *119*(4), 2797-2818. doi: 10.1002/2013JA019542

Vörös, Z., Yordanova, E., Echim, M. M., Consolini, G., & Narita, Y. (2016). Turbulence-generated Proton-scale Structures in the Terrestrial Magnetosheath. , *819*(1), L15. doi: 10.3847/2041-8205/819/1/L15